Physics of Quantum dot junction transistor

Yia-Chung Chang (張亞中)
Research Center for Applied Sciences (RCAS)
Academia Sinica, Taiwan
（中研院 應用科學研究中心）

Collaborators:

C. M.-T. Kuo (郭明庭)(NCU)
S. Sun (UIUC)
Cheche (RCAS)
David Ting (丁肇酉)(JPL)

Applications of QD devices

- Single-electron transistor (SET)
- Single-photon generator (SPG)
- Light-emitting transistor
- Optical signal control (slow light)
- QD lasers & detectors
- Non-linear optical devices
- High-density memory
- Biosensors
- Spintronics devices

Theoretical approaches for one-particle states

- Envelope Function approximation
- K.p theory --
  Effective-mass model (for spherical conduction Band)
  Luttinger model (for degenerate valence bands)
- Effective bond-orbital model
- VFF model (for strain distribution)
- Tight-binding model
- Density-functional theory (DFT)

Physical effects

Quantum confinement (size effect)

Selection rule (light polarization)

Discrete energy levels (0-d density of states)

Strong Coulomb interaction (Coulomb blockade)

Strong electron correlation (many-body effect)

Artificial atom

Self assembled quantum dots

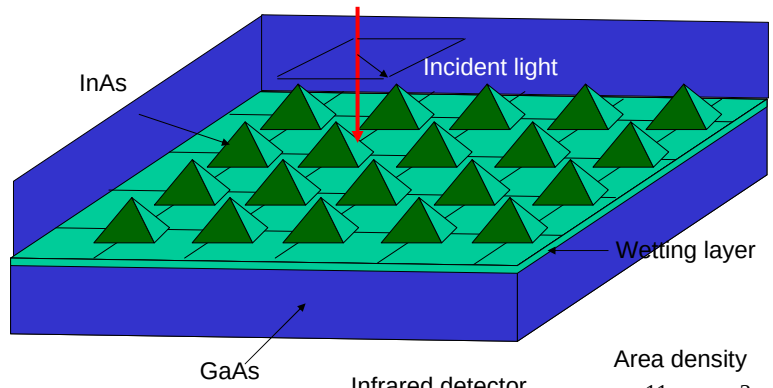

Lattice mismatch 7%

Infrared detector
Laser

Area density

$10^{11} / cm^2$

Optical and Structural Characterization of QDIPs

TEM GaAs

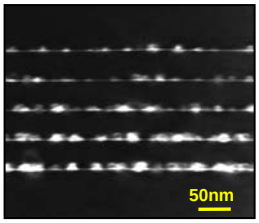

TEM AlGaAs

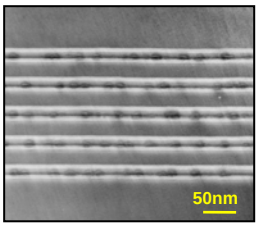

Energies of transitions (from PL/PLE data):
65meV, 89meV
139meV, 195meV

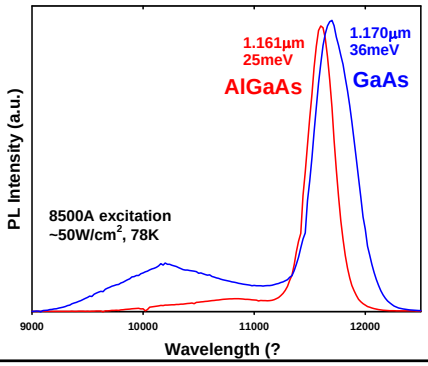

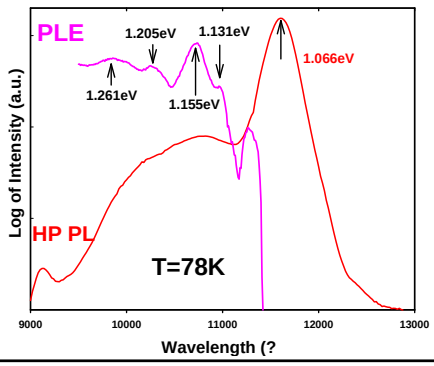

紅外線偵測器 (Infrared detector)

量子井紅外線偵測器(QWIP)

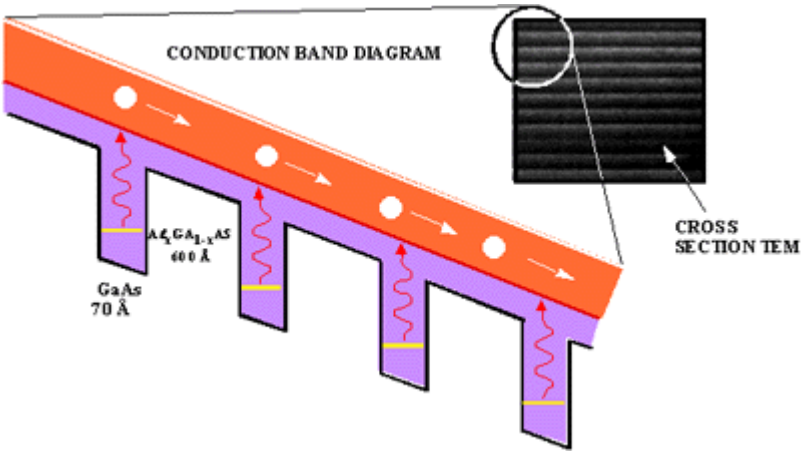

http://qwip.jpl.nasa.gov/tutorial.html

量子井紅外線偵測器 (QWIP)

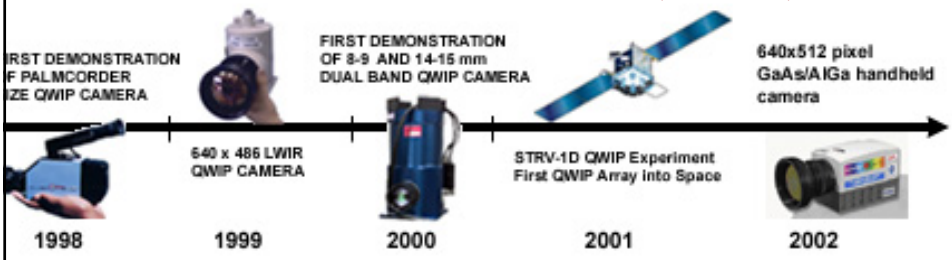

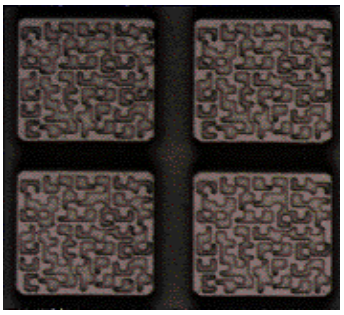

http://qwip.jpl.nasa.gov/tutorial.html

Schematics of QDIP test structures

[Z. Chen and A. Madhukar (USC)]

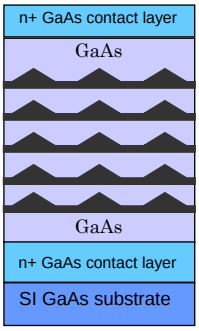

Doping: Balance between PC & Dark Current
n-i(MQD)-n
n-n(MQD)-n

5 layers of
PIG 3ML InAs QDs:
(2ML + Δt + 1ML)
with 150ML GaAs/AlGaAs spacers

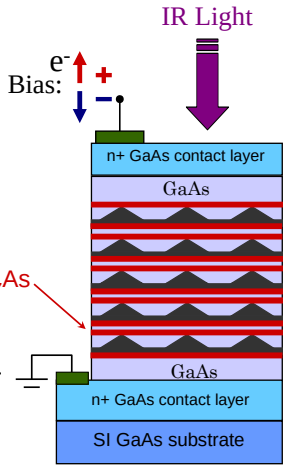

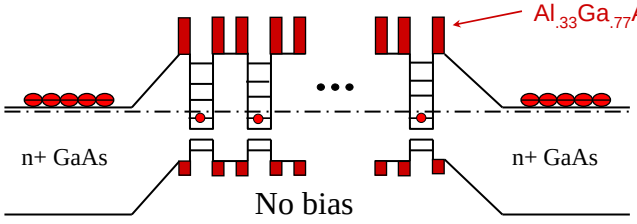

No bias

Microscopic modeling

[S. Sun,Y. C. Chang, PRB 62, 13631 (2000)]

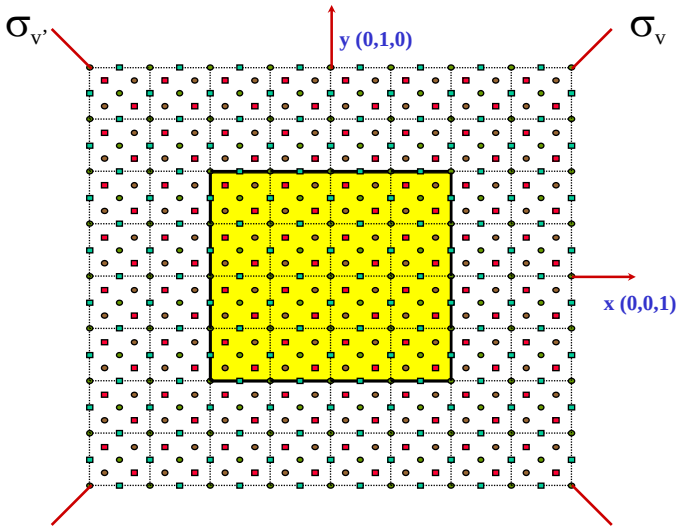

Valence force field (VFF) Model

$$V = \frac{1}{4}\sum_{ij}\frac{3}{4}\alpha_{ij}\left(d_{ij}^2 - d_{0,ij}^2\right)^2 \Big/ d_{0,ij}^2$$

$$+\frac{1}{4}\sum_{i}\sum_{j\neq k}\frac{3}{4}\beta_{ijk}\left(\vec{d}_{ij}\cdot\vec{d}_{ik} + d_{0,ij}d_{0,ik}/3\right)^2 \Big/ d_{0,ij}d_{0,ii}$$

i labels atom positions
j , k label nearest-neighbors of i
d_{ij} = bond length joining sites i and j
$d_{0,ij}$ is the corresponding equilibrium length
α_{ij}= bond stretching constants
d_{ijk}= bond bending constants
We take $d_{ijk}^2 = d_{ij}d_{ik}$

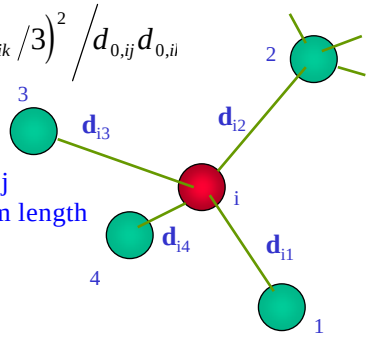

Strain Potential Along Line A and B of Dot 1

UNIVERSITY OF ILLINOIS AT URBANA-CHAMPAIGN

- **Fig.(a):** strain potential along line A
- **Fig.(b):** strain potential along line B

V_{ss}
V_{xx}
V_{yy}
V_{zz}

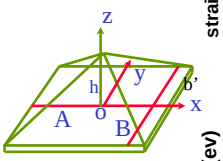

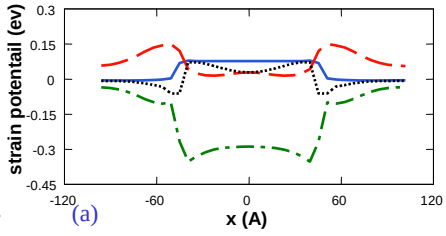

(a)

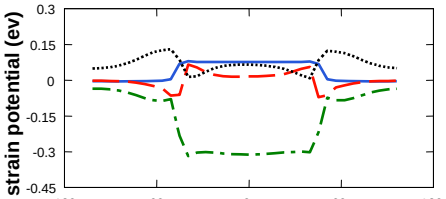

(b)

- **Band offset:**
  CB: 0.833eV
  VB: 0.260eV

Strain Distribution Along [001] of Dot 1 and Dot 2

UNIVERSITY OF ILLINOIS AT URBANA-CHAMPAIGN

- **Hydrostatic Strain :**
  Dot 1: ——
  Dot 2: ……
- **Biaxial Strain:**
  Dot 1: - - - - - -
  Dot 2: —·—·—
- **[001] is growth direction**
- **Dot 1: 0-62.5 A**
  Dot 2: 0-50A

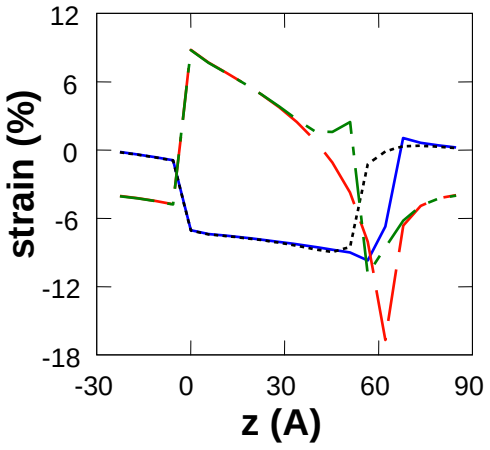

Comparison with continuum Model

J. Appl. Phys. **104**, 083524 (2008)

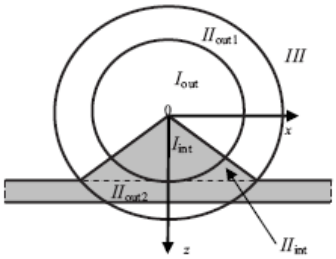

FIG. 1. The schematic representation of the QD-WL system (in gray) in a plan containing *OZ* axes. The specific regions I_{int}, I_{out}, II_{int}, II_{out}, and III are shown.

using Green's function method one obtains (see Refs. 8–10)

$$\mathbf{u}(\mathbf{r}) = \frac{C}{\pi}\oint \frac{1}{|\mathbf{r}-\mathbf{r}_0|} d\mathbf{S}(\mathbf{r}_0), \quad (1)$$

where $C=\varepsilon_d(1+\nu)/[4(1-\nu)]$, ν is Poisson's ratio,[13] ε_d is the interface dilation defined as $\varepsilon_d=(a_{int}-a_{ext})/a_{ext}$ (a_{ext}, a_{int} are the lattice constant of the external, internal (inclusion) material, respectively) and it coincides with the *compression*

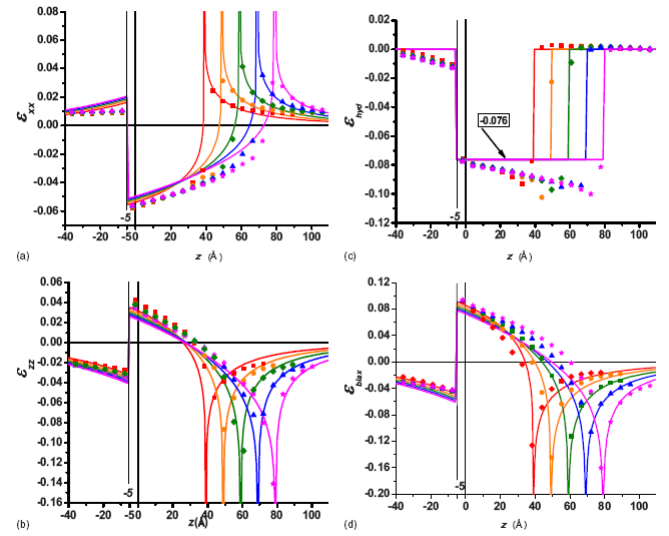

FIG. 3. (Color online) The strains on *OZ* axes: (a) the radial strain ε_{xx}, (b) the strain ε_{zz}, (c) the hydrostatic ε_{hyd}, and (d) the biaxial strain ε_{bias} on the *OZ* axis, for the ratios R/H=10/3.9, 10/4.9, 10/5.9, 10/6.9, 10/7.9, with R=100 Å. The dots are for the VFF model and the continuum lines for CM.

Piezoeletric Potential

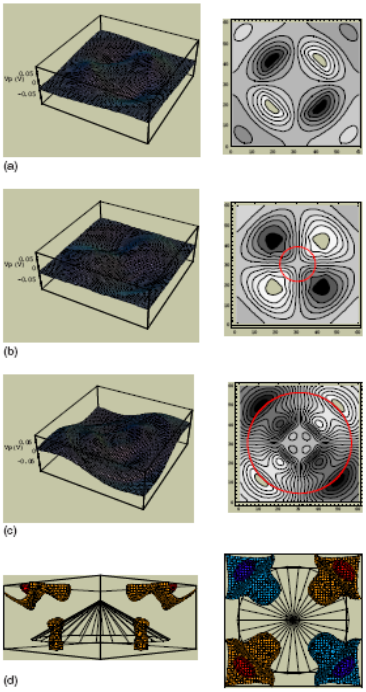

FIG. 5. (Color online) The piezoelectric potential V_p: (a) in the horizontal plane, $z=0$ containing the top of the cone; (b) in the horizontal plan $z=H/3$; (c) in the horizontal plane $z=H$. The left side figures are the three-dimensional plots and the right side figures are the contour plots. The red circles in these plots represent the cross sections of the QD with the horizontal planes. (d) equipotential surfaces of piezoelectric potential V_p for 0.065 V (red), −0.065 V (dark blue), 0.04 V (orange), and −0.04 V (blue). In the left side figure only the positive equipotential surfaces are plotted. In the right side figure are plots with a top view.

Effective bond-orbital Model
[Y.C.Chang, PRB 37, 8215 (1988)]

UNIVERSITY OF ILLINOIS AT URBANA-CHAMPAIGN

$$H_{\alpha,\alpha'}(\vec{k}) = E_p \delta_{\alpha,\alpha'} + \sum_{\vec{\tau}} e^{i\vec{k}\cdot\vec{\tau}} \left\{ E_{xy} \tau_\alpha \tau_{\alpha'} + \left[\left(E_{xx} - E_{xy} \right) \tau_\alpha^2 + E_{zz} \left(1 - \tau_\alpha^2 \right) \right] \delta_{\alpha,\alpha'} \right.$$

Strain Hamiltonian

$$H_{st} = \begin{pmatrix} -\Delta V_H + D_1 & \sqrt{3} d e_{xy} & \sqrt{3} d e_{xz} \\ \sqrt{3} d e_{xy} & -\Delta V_H + D_2 & \sqrt{3} d e_{yz} \\ \sqrt{3} d e_{xz} & \sqrt{3} d e_{yz} & -\Delta V_H + D_3 \end{pmatrix}$$

$e_{ij}=(\varepsilon_{ij}+\varepsilon_{ji})/2$
$\Delta V_H=(a_1+a_2)(\varepsilon_{xx}+\varepsilon_{yy}+\varepsilon_{zz})$
$D_1=b(2\varepsilon_{xx}-\varepsilon_{yy}-\varepsilon_{zz})$
$D_2=b(2\varepsilon_{yy}-\varepsilon_{xx}-\varepsilon_{zz})$
$D_3=b(2\varepsilon_{zz}-\varepsilon_{xx}-\varepsilon_{yy})$
a_1, a_2, b, d = deformation potentials.

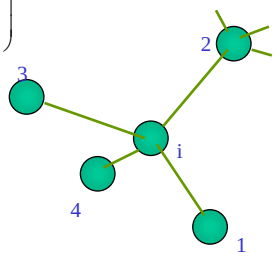

Ground Transition Energy Varying With Dot Height (comparing to Experiment)

UNIVERSITY OF ILLINOIS AT URBANA-CHAMPAIGN

Dot base length 200Å

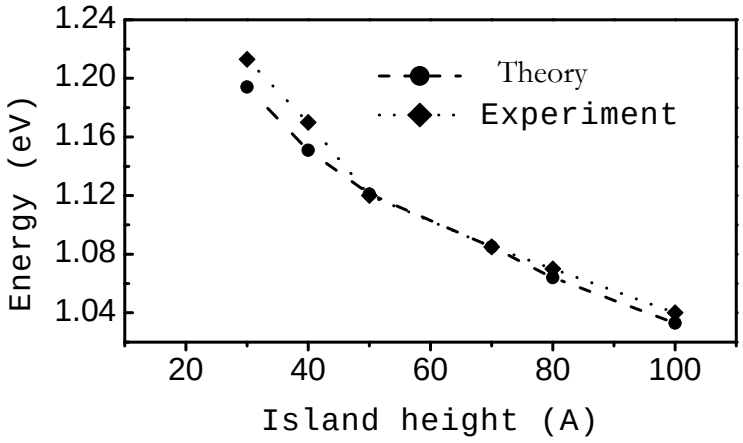

PL/PLE Characterization: Electronic Structure

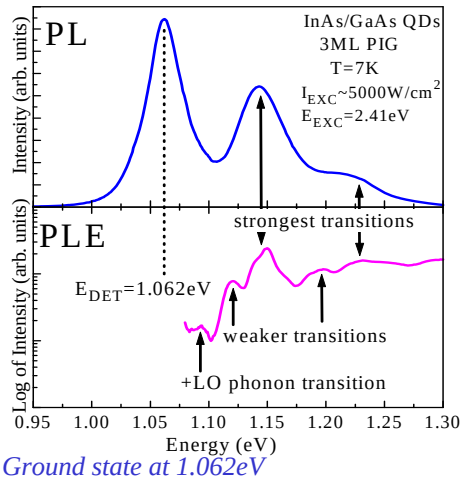

Ground state at 1.062eV

Excited states:

Strongest at 1.147eV and 1.229eV

Weaker at 1.121eV and 1.197eV

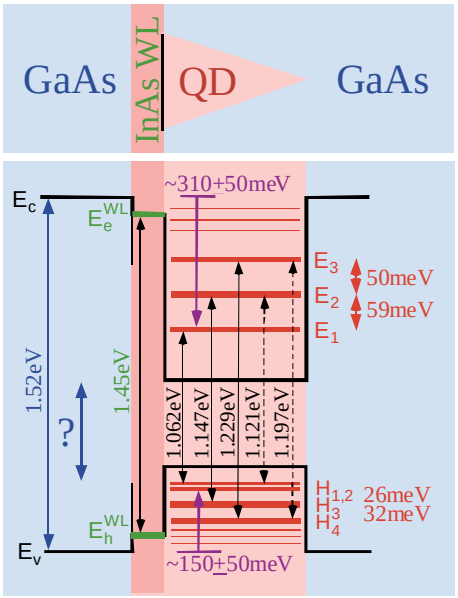

Intra-band Transitions

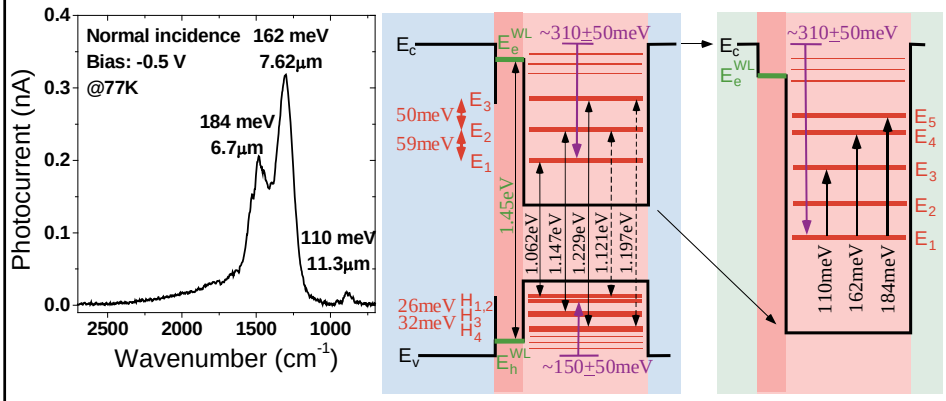

A. Madhkar (USC)

Intra-band Transitions

Table 4 Inter-sub band transition matrix elements of ground electron state to upper three electron states, $\left|\langle\phi_{i,c}|r|\phi_{i,c}\rangle\right|^2$. B=200A, h=80A.

Symmetry	state i	x	y	z
A1	#2 (0.111)	0	0	0.2
	#3 (0.123)	0	0	57
	#4 (0.197)	0	0	201
A2	#2 (0.106)	0	0	28.5
	#3 (0.114)	0	0	0
B1,B2	#2 (0.109)	0	0	15
	#3 (0.138)	0	0	42
	#4 (0.201)	0	0	14
A1-B1n	#1 (0.062)	446	446	0
	#2 (0.162)	0.2	0.2	0
	#3 (0.218)	0.4	0.4	0
B1-A1n	#2(0.049)	536	536	0
	#3(0.061)	659	659	0
	#4(0.135)	376	376	0
	#5(0.161)	10.2	10.2	0

Theoretical Analysis

- Energy and wave functions computed using a stabilized transfer matrix technique by dividing the system into many slices along growth direction.
- Envelope function approximation with energy-dependent effective mass is used.
- Effective-mass Hamiltonian in k-sapce:

$$[(k_x^2+k_y^2)/m_t(E)+\partial_z^2/m_l(E)-E]F(\mathbf{k}) + \sum_{\mathbf{k}'}[V(\mathbf{k},\mathbf{k}')+V_{imp}(\mathbf{k},\mathbf{k}')]F(\mathbf{k}')=0$$

  is solved via plane-wave expansion in each slice.
- 14-band k·p effects included perturbatively in optical matrix elements calculation
- Dopant effects incorporated as screened Coulomb potential
- The technique applies to quantum wells and quantum dots (or any 2D periodic nanostructures)

Charge densities of low-lying states in lens-shaped QD

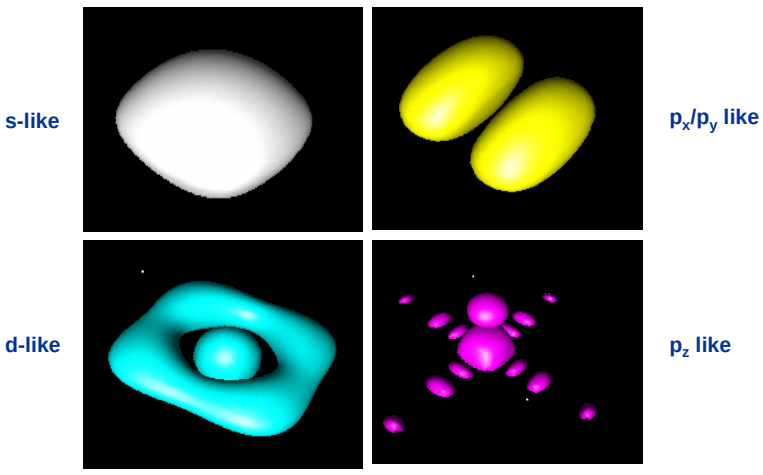

Quantum well intrasubband photodetector (QWISP) for far infared and terahertz radiation detection

[Ting et al., APPLIED PHYSICS LETTERS 91, 073510 (2007)]

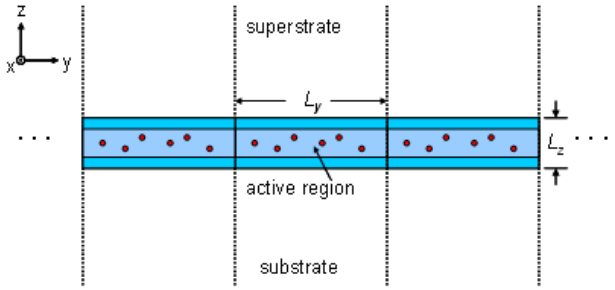

Fig. 4 A schematic illustration of the laterally repeating supercell geometry used in our simulations. Note that the supercell also repeats in the *x* direction with periodicity of L_x (not drawn). The example shown in this figure illustrates a quantum well containing several randomly placed dopant impurities.

Quantum well intrasubband photodetector (QWISP) for far infared and terahertz radiation detection

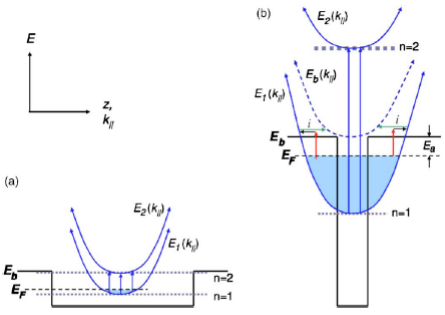

FIG. 1. (Color online) Schematic illustrations of the energy dispersions and energy band diagrams of (a) FIR/terahertz QWIP; (b) QWISP showing intersubband and impurity scattering assisted intrasubband optical absorption and carrier extraction mechanisms.

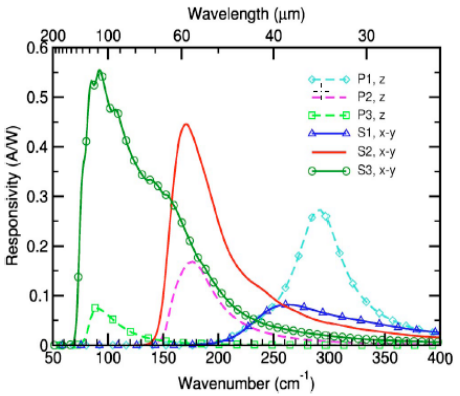

FIG. 3. (Color online) Low-temperature FIR/terahertz QWIP (set P) side-incidence responsivity and QWISP (set S) normal-incidence responsivity. Modeling parameters are listed in Table I.

Quantum well intrasubband photodetector (QWISP) for far infared and terahertz radiation detection

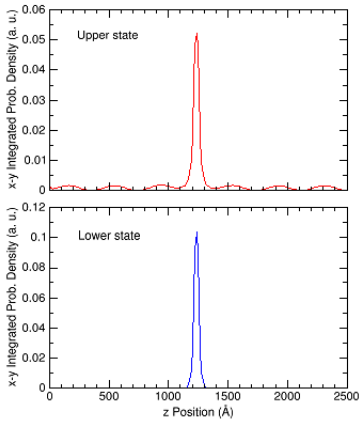

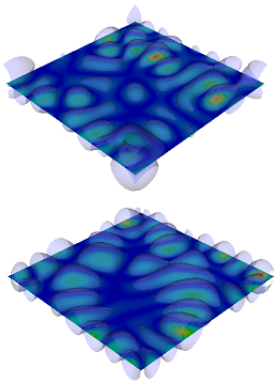

Fig. 5 The zero-bias wave functions of a pair of states involved in an intra-subband transition in a QWISP structure. The energy of the lower state is slightly below the Fermi level, and the energy of the upper state is just above the barrier band edge. The left panel shows the in-plane averaged probability densities as functions of z (growth direction). The random dopant distribution induced in-plane fluctuations of the wave functions are displayed in the right panel, which shows the translucent probability density isosurfaces, overlaid on top of probability density color contour plane located at the middle of the quantum well.

Submonolayer QD infrared photodetector

[Ting et al., APPLIED PHYSICS LETTERS 94, 1 (2009)]

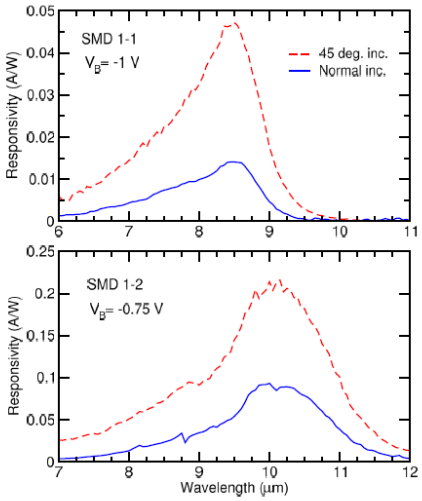

FIG. 2. (Color online) Measured normal and 45° incidence spectral responsivity curves for two SML QDIP samples.

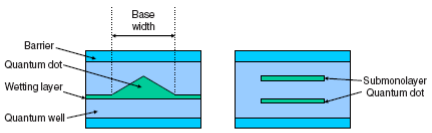

FIG. 1. (Color online) The left panel illustrates a conventional DWELL structure where a SK QD, consisting of pyramidal shape QD resting on a wetting layer, is embedded in a QW structure. The right panel show two stacks of SML QDs embedded in a QW.

FIG. 4. (Color online) 80 K images taken with a 1024×1024 pixel SML QDIP FPA with $f/2$ optics.

Principle of the SET transistor

Like a MOSFET, the single-electron tunnelling (SET) transistor consists of a gate electrode that electrostatically influences electrons travelling between the source and drain electrodes. However, the electrons in the SET transistor need to cross two tunnel junctions that form an isolated conducting electrode called the island. Electrons passing through the island charge and discharge it, and the relative energies of systems containing 0 or 1 extra electrons depends on the gate voltage.

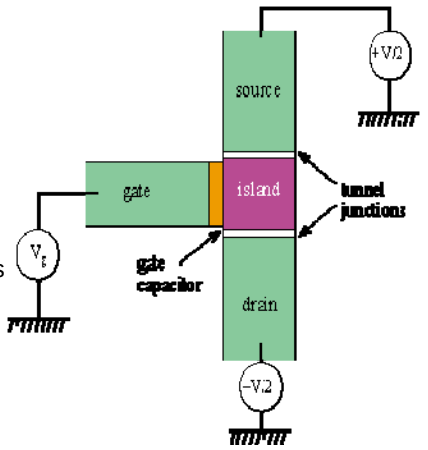

Single-electron transistor (SET)

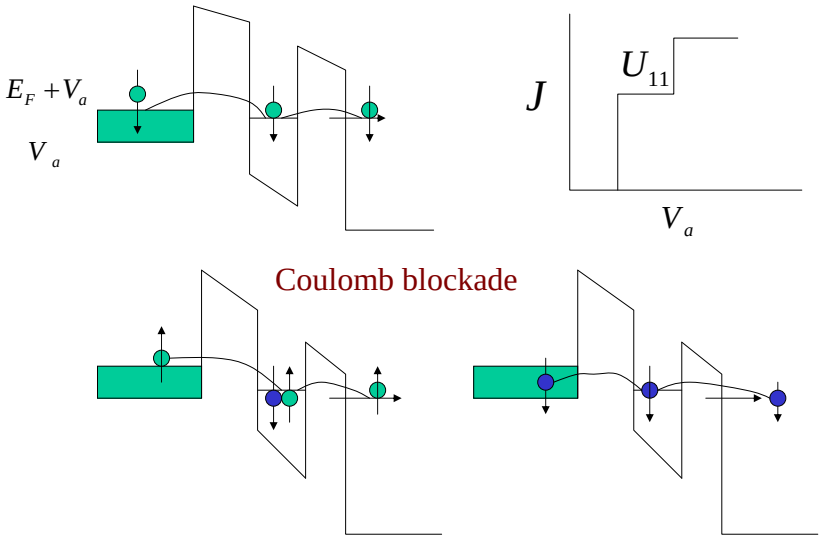

Tunneling current with Coulomb blockade

$$J = \frac{2e}{h}\sum_{\alpha}\int dw\Gamma[\, f_L(w-\mu_L) - f_R(w-\mu_R)]\,\mathrm{Im}\,G_{d\alpha}(w)$$

$$G_{d\alpha}(w) = [\frac{1-\langle n_{d,\alpha}\rangle}{w-\varepsilon_0+i\Gamma} + \frac{\langle n_{d,\alpha}\rangle}{w-\varepsilon_0-U\ \ +i\Gamma}]$$

$$\langle n_{d,-\alpha}\rangle = \langle n_{d,\alpha}\rangle = \frac{1}{\pi}\int_{-\infty}^{\infty} dw \frac{f_L(w-\mu_L)+ f_R(w-\mu_R)}{2}\,\mathrm{Im}\,G_{d\alpha}(w)$$

CdSe nanoparticles

(as fluorescent tags for biochemical analysis)

average diameter of particles (nm)

2.4 2.8 3.4 3.8 4.2

Fluorescence from Nanoparticles of Various Diameters

http://unit.aist.go.jp/kyushu/mischel/eng/theme/theme2.htm

Tunneling current spectroscopy of a nanostructure junction involving multiple energy levels

David M T Kuo & Y. C. Chang

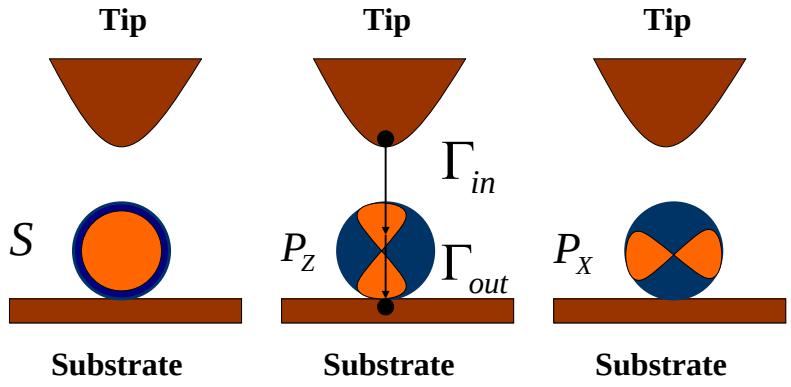

E_s, E_{p_z}, E_d

P. Liljeroth et al, Phys. Chem.chem. Phys. 8, 3845 (2006)

Energy diagram for STM-QD junction

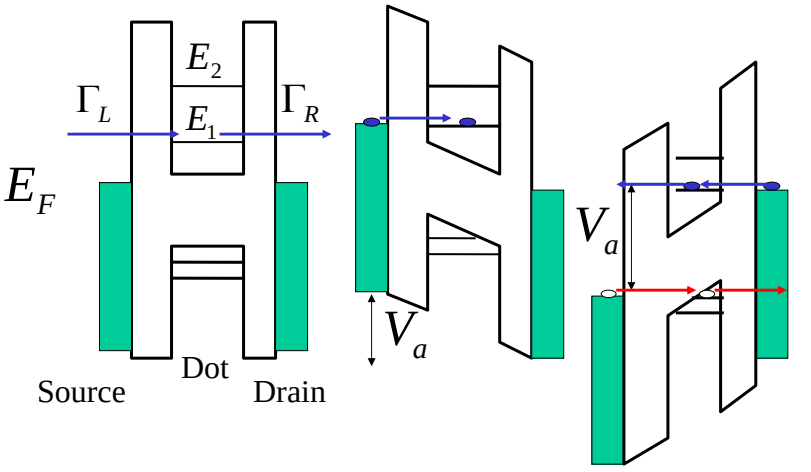

(a) No bias (b) Forward bias (c) Reverse bias

Experimental results

- Differential conductance oscillation

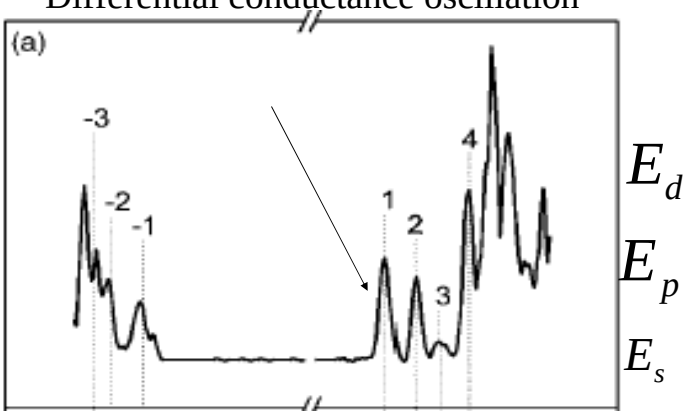

Identify current spectra.

L. Jdira et al, Phys. Rev. B 73, 115305 (2006)

Multi-level Anderson Hamiltonian

$$H = \sum_{k,\sigma,\beta} \epsilon_k a^\dagger_{k,\sigma,\beta} a_{k,\sigma,\beta} + \sum_{\ell,\sigma} E_\ell d^\dagger_{\ell,\sigma} d_{\ell,\sigma} \qquad (1)$$
$$+ \sum_{\ell,j,\sigma,\sigma'} U_{\ell,j} d^\dagger_{\ell,\sigma} d_{\ell,\sigma} d^\dagger_{j,\sigma'} d_{j,\sigma'} + \sum_{k,\sigma,\beta,\ell} V_{k,\beta,\ell} a^\dagger_{k,\sigma,\beta} d_{\ell,\sigma}$$
$$+ \sum_{k,\sigma,\beta,\ell} V^*_{k,\beta,\ell} d^\dagger_{\ell,\sigma} a_{k,\sigma,\beta}$$

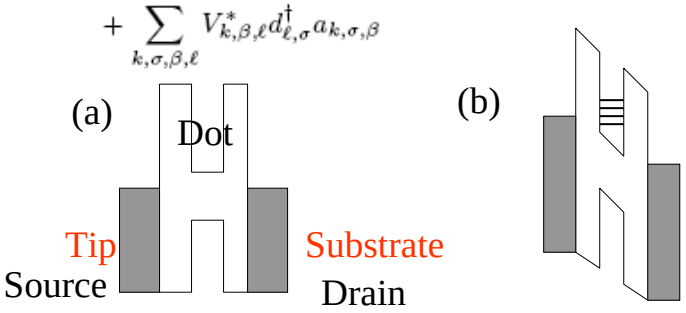

H. Haug and A. P. Jauho, *Quantum Kinetics in Transport and Optics of Semiconductor* (Springer, Heidelberg, 1996).

Tunneling Current formula

$$J = \frac{-2e}{\hbar}\sum_{\ell}\int \frac{d\epsilon}{2\pi}[f_{in}(\epsilon-\mu_{in}) - f_{out}(\epsilon-\mu_{out})] \qquad (2)$$

$$\frac{\Gamma_{\ell,in}(\epsilon)\Gamma_{\ell,out}(\epsilon)}{\Gamma_{\ell,in}(\epsilon)+\Gamma_{\ell,out}(\epsilon)} Im G^{r}_{\ell,\sigma}(\epsilon),$$

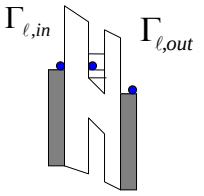

Is it possible to have a simple, efficient and reliable spectral function for a QD with arbitrary number of energy levels to determine the electronic structure of a single QD?

H. Haug and A. P. Jauho, *Quantum Kinetics in Transport and Optics of Semiconductor* (Springer, Heidelberg, 1996).

Mean-field approximation

$< d_{i\sigma}{}^{+}d_{i\sigma}\ d_{j\sigma},{}^{+}d_{j\sigma}, > = < d_{i\sigma}{}^{+}d_{i\sigma} >< d_{j\sigma},{}^{+}d_{j\sigma}, >$ for $i \neq j$

- **One level case**

$$G^{r}_{1,\sigma} = (1-N_{1,-\sigma})\left(\frac{1}{\varepsilon - E_1 + i\frac{\Gamma_1}{2}}\right) + N_{1,-\sigma}\left(\frac{1}{\varepsilon - E_1 - U_1 + i\frac{\Gamma_1}{2}}\right)$$

The mean-field approximation is adequate for describing the Coulomb blockade, but not the Kondo effect

$N_1 = \langle d^{+}d \rangle$ is the average one-particle occupation number, which determines the probability of each resonant level.

How about the expression of retarded Green's functions for two-level, three-level and n-level case ?

H. Haug and A. P. Jauho, *Quantum Kinetics in Transport and Optics of Semiconductor* (Springer, Heidelberg, 1996).

Two-level case (n=2)

$$G^{r}_{\ell,\sigma}(\varepsilon) = (1 - N_{\ell,-\sigma}) \sum_{m=1}^{3} \frac{p_m}{\varepsilon - E_\ell - \Pi_m + i\frac{\Gamma_\ell}{2}} + N_{\ell,-\sigma} \sum_{m=1}^{3} \frac{p_m}{\varepsilon - E_\ell - U_\ell - \Pi_m + i\frac{\Gamma_\ell}{2}}$$

Probability factors	Interlevel Coulomb factors
$p_1 = a^j \equiv 1-(N_{j,\sigma}+N_{j,-\sigma})+\langle n_{j\sigma}n_{j-\sigma}\rangle$	$\Pi_1 = 0$
$p_2 = b^j \equiv N_{j,\sigma}+N_{j,-\sigma}-2\langle n_{j\sigma}n_{j-\sigma}\rangle$	$\Pi_2 = U_{\ell j}$
$p_3 = c^j \equiv \langle n_{j\sigma}n_{j-\sigma}\rangle$	$\Pi_3 = 2U_{\ell j}$
$\ell \neq j$	

M-level case

$a^j \equiv 1-(N_{j,\sigma}+N_{j,-\sigma})+\langle n_{j\sigma}n_{j-\sigma}\rangle$

$b^j \equiv N_{j,\sigma}+N_{j,-\sigma}-2\langle n_{j\sigma}n_{j-\sigma}\rangle$

$c^j \equiv \langle n_{j\sigma}n_{j-\sigma}\rangle$

$\ell \neq j \neq j'$

$a^{j'} \equiv 1-(N_{j',\sigma}+N_{j',-\sigma})+\langle n_{j'\sigma}n_{j'-\sigma}\rangle$

$b^{j'} \equiv N_{j',\sigma}+N_{j',-\sigma}-2\langle n_{j'\sigma}n_{j'-\sigma}\rangle$

$c^{j'} \equiv \langle n_{j'\sigma}n_{j'-\sigma}\rangle$

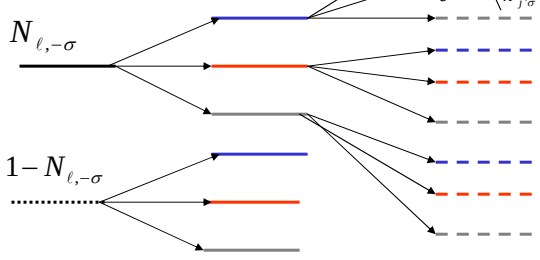

$p_1 = a^j a^{j'},\ p_2 = b^j a^{j'},\ p_3 = a^j b^{j'},\ p_4 = c^j a^{j'},\ p_5 = c^{j'} a^j, ..$

$\Pi_1 = 0, \Pi_2 = U_{\ell j}, \Pi_3 = U_{\ell j'}, \Pi_4 = 2U_{\ell j}, \Pi_5 = 2U_{\ell j'},$

We define the $(2+n)$- and $(1+n)$-particle ($n \leq 2M-2$) Green's functions as

$$G^r_{\ell,\ell,j_1,\cdots j_n} = \langle n_{\ell,-\sigma} n_{j_1} \cdots n_{j_n} d_{\ell,\sigma} d^\dagger_{\ell,\sigma} \rangle$$

and

$$G^r_{\ell,j_1,\cdots j_n} = \langle n_{j_1} \cdots n_{j_n} d_{\ell,\sigma} d^\dagger_{\ell,\sigma} \rangle,$$

where $j_1, \cdots j_n$ label any n states out of the $2(M-1)$ states (excluding spin up and down states in level ℓ). Here j_α is a composite index for energy level and spin. In general, the $(2+n)$- and $(1+n)$-particle ($n \leq 2M-2$) Green's functions satisfy

$$(\mu_l - U_\ell - \sum_{\alpha=1}^{n} U_{\ell j_\alpha}) G^r_{\ell,\ell,j_1,\cdots j_n} = N_{\ell,-\sigma} \langle n_{j_1} \cdots n_{j_n} \rangle + \sum_{j'}^{''} U_{\ell,j'} G^r_{\ell,\ell,j_1,\cdots j_n,j'}, \quad (32)$$

and

$$(\mu_l - \sum_{\alpha=1}^{n} U_{\ell j_\alpha}) G^r_{\ell,j_1,\cdots j_n} = \langle n_{j_1} \cdots n_{j_n} \rangle + U_\ell G^r_{\ell,\ell,j_1,\cdots,j_n} + \sum_{j'}^{''} U_{\ell,j'} G^r_{\ell,j_1,\cdots j_n,j'}, \quad (33)$$

where the "double prime" on the summation indicates that j' is not among the n states and not in the level ℓ. In the n-particle state labeled by $j_1, \cdots, j_n$ if there are m levels occupied with two particles and the rest singly occupied, we can label them by $j_1, j_1, \cdots, j_m, j_m, j_{2m+1}, \cdots, j_n$. We then assume that the n-particle correlation function can

$$G^r_{2M} = \frac{N_{\ell,-\sigma} \prod'_j c_j}{(\mu_l - U_\ell - 2\sum'_j U_{\ell,j})}, \quad (4)$$

where $\mu_\ell \equiv \epsilon - E_\ell + i(\Gamma_{\ell,L} + \Gamma_{\ell,R})/2$ and $U_{\ell,j}$ denotes the on-site Coulomb energy in level ℓ. $N_{j,-\sigma} = \langle n_{j,-\sigma} \rangle$ and $c_j = \langle n_{j,-\sigma} n_{j,\sigma} \rangle$ denote the one-particle and two-particle average occupancy in the level j. Here and henceforth, $\prod'_j$ means taking the product of terms labeled by j with $j = 1, \cdots M$, excluding ℓ.

$$G^r_{\ell,\ell}(\epsilon) = \prod_j^{'} (\hat{a}_j + \hat{b}_j + c_j) G^r_{2M} / \prod_j^{'} c_j \equiv N_{\ell,-\sigma} \sum_{m=1}^{3^{M-1}} \frac{p_m}{\mu_\ell - U_\ell - \Pi_m} \quad (5)$$

and

$$G^r_{\ell,\sigma}(\epsilon) = (\hat{b}_\ell N^{-1}_{\ell,-\sigma} + 1) G^r_{\ell,\ell}(\epsilon) \quad (6)$$
$$= (1 - N_{\ell,-\sigma}) \sum_{m=1}^{3^{M-1}} \frac{p_m}{\mu_\ell - \Pi_m} + N_{\ell,-\sigma} \sum_{m=1}^{3^{M-1}} \frac{p_m}{\mu_\ell - U_\ell - \Pi_m},$$

where $\hat{b}_\ell$, $\hat{a}_j$, and $\hat{b}_j$ are operators that put a factor $b_\ell = 1 - N_{\ell,-\sigma}$, $a_j \equiv 1 - (N_{j,\sigma} + N_{j,-\sigma}) + c_j$, and $b_j \equiv N_{j,\sigma} + N_{j,-\sigma} - 2c_j$ in the numerator and increases the value of the denominator by U_ℓ, $2U_{\ell,j}$ and $U_{\ell,j}$, respectively when acting on a fractional function. For ex-

Differential conductance dJ/dV is determined by:

$$G^r_{\ell,\sigma}(\epsilon) = (1 - N_{\ell,-\sigma}) \sum_{m=1}^{3^{n-1}} \frac{p_m}{\epsilon - E_\ell - \Pi_m + i\frac{\Gamma_\ell}{2}} + N_{\ell,-\sigma} \sum_{m=1}^{3^{n-1}} \frac{p_m}{\epsilon - E_\ell - U_\ell - \Pi_m + i\frac{\Gamma_\ell}{2}},$$

Π_m = sum of Coulomb interactionsin configuration m.

p_m = probability of finding the system in configuration m.

Level $j(j \neq \ell)$ can be occupied by 0, 1 or 2 particles.

For a two-level $(n = 2)$ system $(\ell \neq j)$, we have three configurations:

$p_1 = a^j \equiv 1 - (N_{j,\sigma} + N_{j,-\sigma}) + \langle n_{j,\sigma} n_{j,-\sigma} \rangle$

(the probability with no particle in level j).

$p_2 = b^j \equiv N_{j,\sigma} + N_{j,-\sigma} - 2\langle n_{j,\sigma} n_{j,-\sigma} \rangle$

(the probability with one particle in level j)

$p_3 = c^j \equiv \langle n_{j,\sigma} n_{j,-\sigma} \rangle$

(the probability with two particles in level j)

$\Pi_1 = 0$, $\Pi_2 = U_{\ell j}$ and $\Pi_3 = 2U_{\ell j}$.

$U_{\ell j}$ = Coulomb interaction between level ℓ and level j.

$$p_m = \prod_j{}' (\hat{a}_j + \hat{b}_j + c_j)$$

2. Three-level system at symmetry case

Based on three-level case

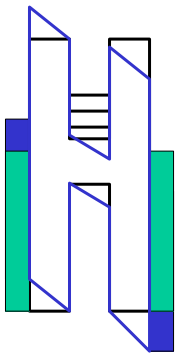

Metal **Metal**

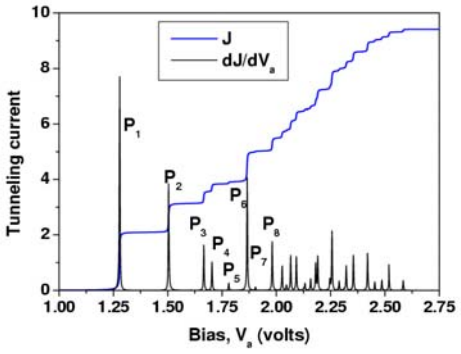

At zero temperature

- d-orbital

Asymmetry tunneling rates

- Tunneling rates Γ_{in} and Γ_{out}

(a) **Shell tunneling** (b) **Shell-filling**

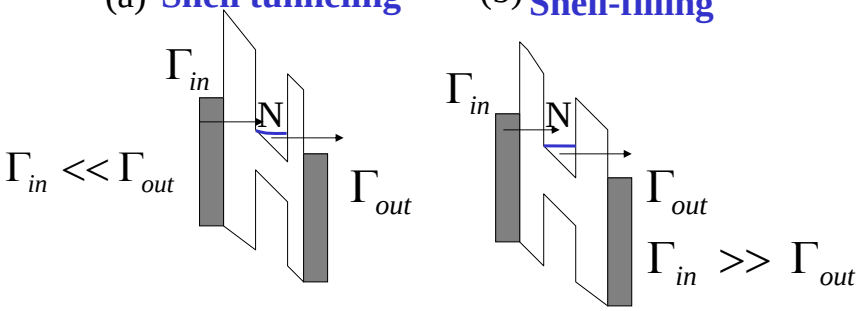

The characteristics of tunneling current of junctions can be classified into either the shell-tunneling case (no charge accumulation) or the shell-filling case (with charge accumulation)

Effect of asymmetric tunneling

$\Gamma_{out} = 1meV$

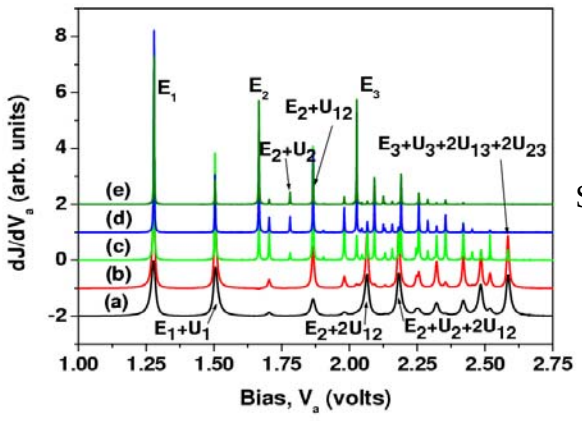

$\Gamma_{in} = 0.1meV$
Shell-tunneling

Shell-filling
$\Gamma_{in} = 10meV$

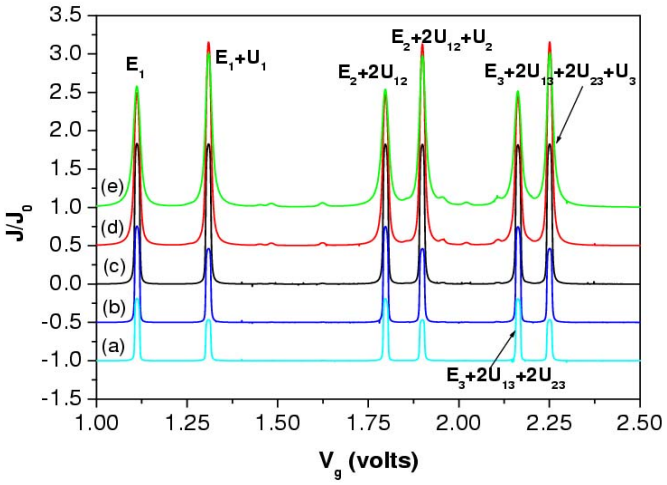

Current versus gate volatge at V_a = 10 mV for various ratios of Γ_L/Γ_R (Γ_R is fixed at 1 meV) :
(a) 0.2, (b) 0.4, (c) 1, (d) 5 and (e) 10.
.

Theory vs. Experiment for STM-QD tunneling spectra

[Data from L. Jdira et al., Phys. Rev. B 73, 115305 (2006)]

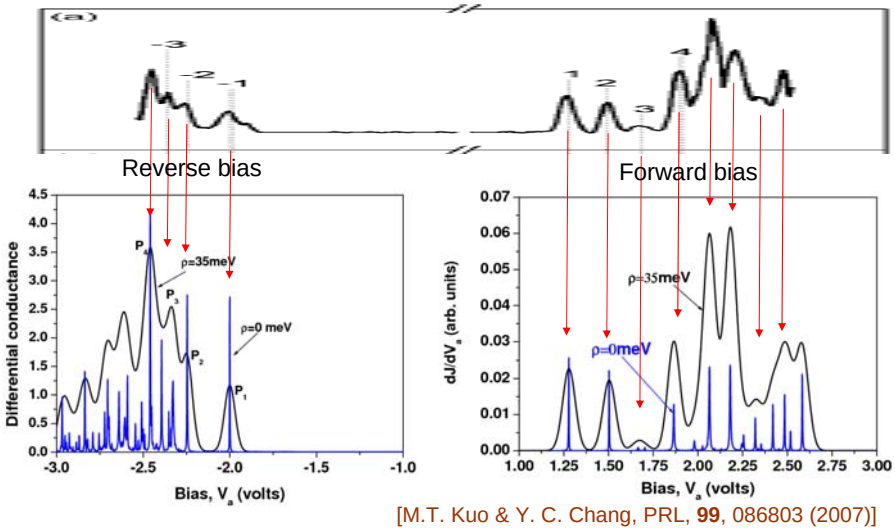

[M.T. Kuo & Y. C. Chang, PRL, **99**, 086803 (2007)]
[Y. C. Chang & M.T. Kuo, PRB, **77**, 245412 (2008)]

Proximity effect for coupled QDs

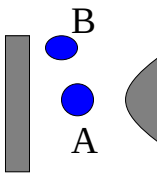

$$\Gamma_{in,A} = 1meV$$
$$\Gamma_{out,A} = 1meV$$
$$\Gamma_{in,B} = 1meV$$
$$\Gamma_{out,B} = 0.1meV$$

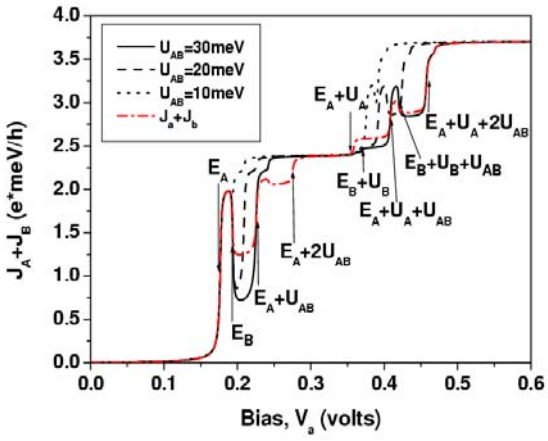

Proximity effect for tunneling current in nanojunction with coupled QDs

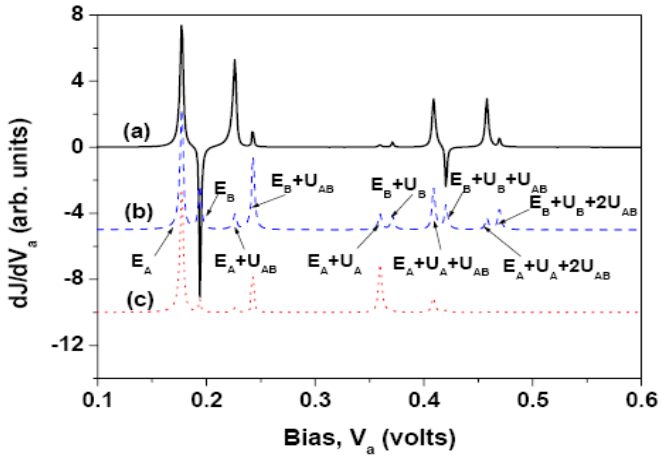

FIG. 4: Differential conductance as a function of applied bias for various tunneling rate ratios of $\Gamma_{L,B}/\Gamma_{R,B}$. U_{AB} = 30 meV. (a) $\Gamma_{L,B}$ = 1 meV and $\Gamma_{R,B}$ = 0.1 meV. (b) $\Gamma_{L,B}$ = 1 meV and $\Gamma_{R,B}$ = 1 meV. (c) $\Gamma_{L,B}$ = 0.1 meV and $\Gamma_{R,B}$ = 1 meV.

Single-Photon generator

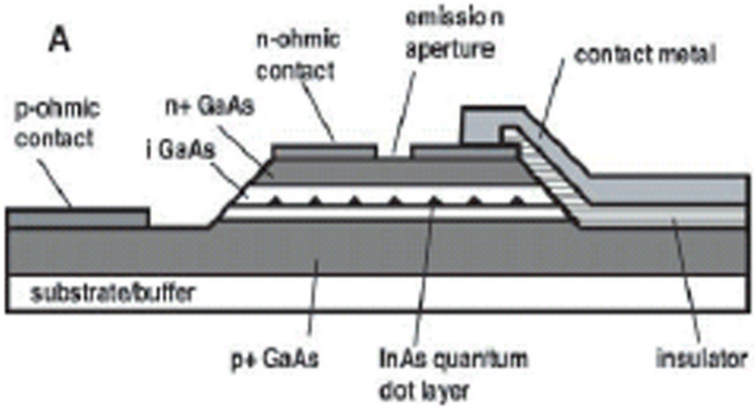

Z. Yuan et al., Science, 295, 102 (2002

Emission spectra of exciton complexes for various applied biases in a reverse bias setup

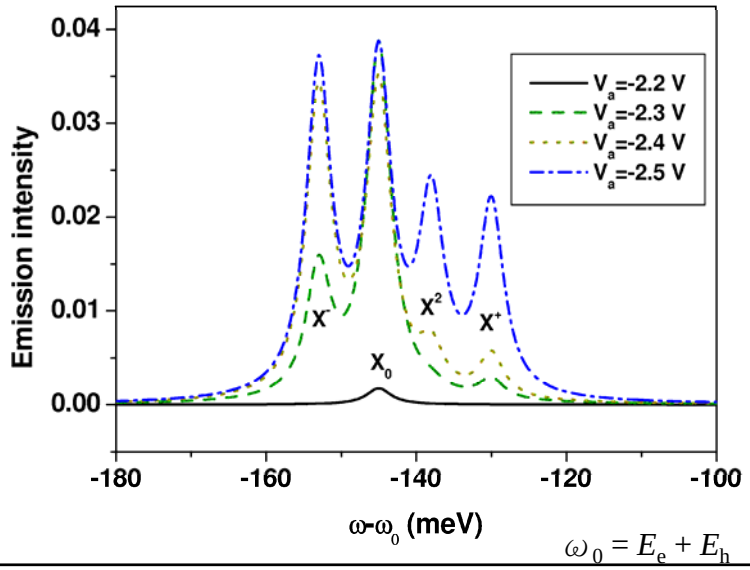

$\omega_0 = E_e + E_h$

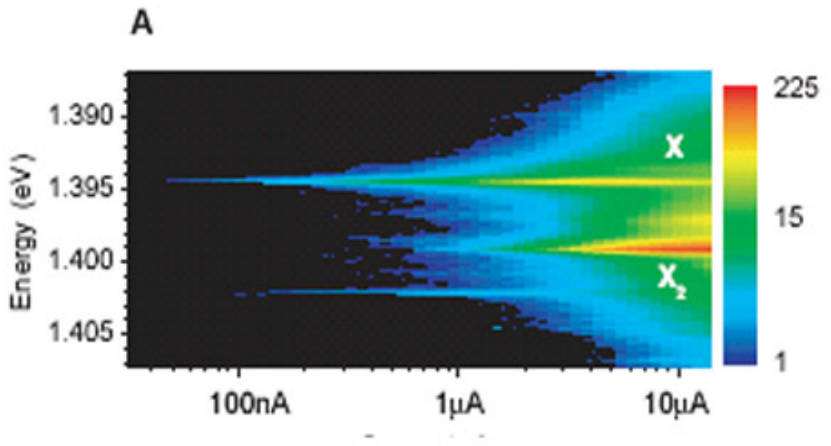

Z. Yuan et al., Science, 295, 102 (2002)

Including optical field

$$\Gamma_1 N_1 = -\mathrm{Im}p - \int \frac{d\varepsilon}{\pi} \Gamma_1^{L/R} f_{L/R}(\varepsilon) \mathrm{Im} G_{11}^r(\varepsilon + \frac{\omega}{2})$$

$$\Gamma_2 N_2 = \mathrm{Im}p - \int \frac{d\varepsilon}{\pi} \Gamma_2^{L/R} f_{L/R}(\varepsilon) \mathrm{Im} G_{22}^r(\varepsilon - \frac{\omega}{2})$$

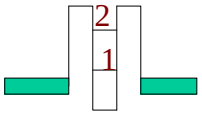

$$\mathrm{Im}p \approx 2\lambda^2 \int \frac{d\varepsilon}{2\pi} \frac{\Gamma_1^L f_L(\varepsilon) + \Gamma_1^R f_R(\varepsilon)}{\Gamma_1} \{ \mathrm{Im}(\frac{1 - N_1}{\varepsilon - E_1 + i\frac{\Gamma_1}{2}}) \mathrm{Im}(\frac{1}{\varepsilon - E_2 + \omega - i\frac{\Gamma_2}{2}})$$

$$+ \mathrm{Im}(\frac{N_1}{\varepsilon - E_1 - U_{11} + i\frac{\Gamma_1}{2}}) \mathrm{Im}(\frac{1}{\varepsilon - E_2 - U_{12} + \omega - i\frac{\Gamma_2}{2}}) \}$$

Coulomb interactions vs. QD size

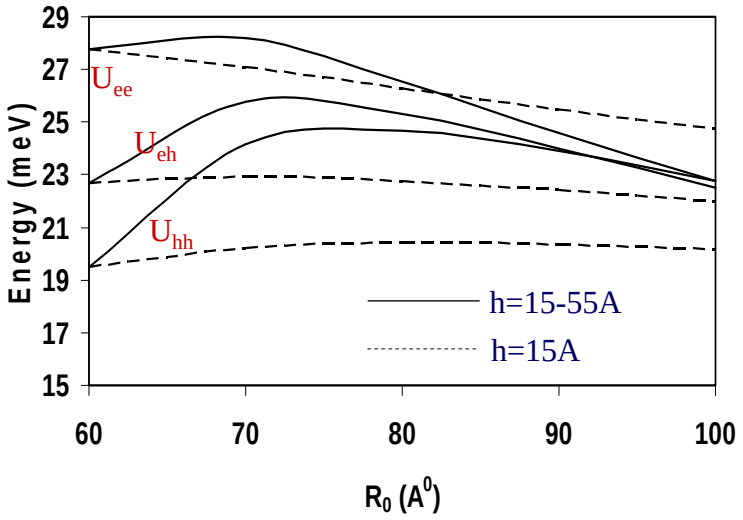

Spontaneous emission spectrum

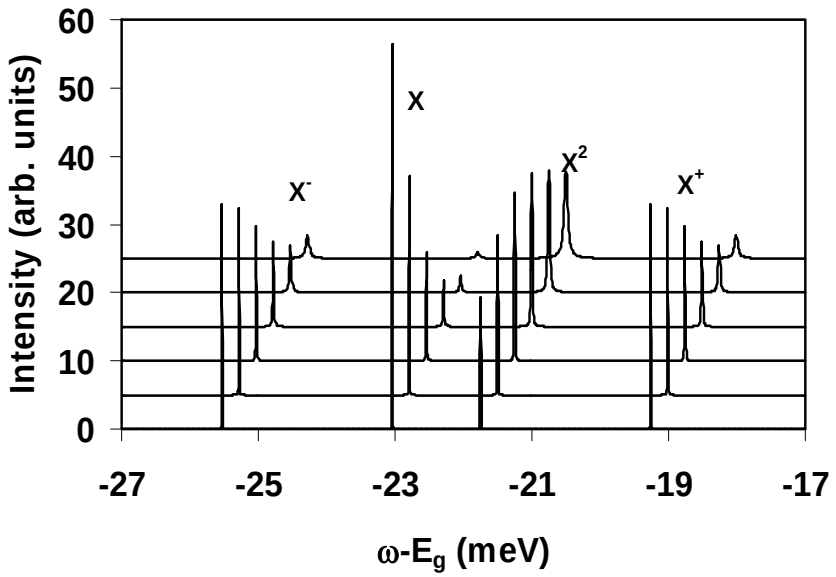

Intensity vs current

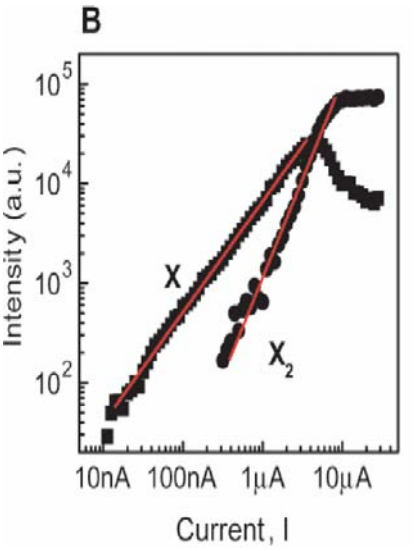

[Z. Yuan et al., Science, 295, 102 (2002)]

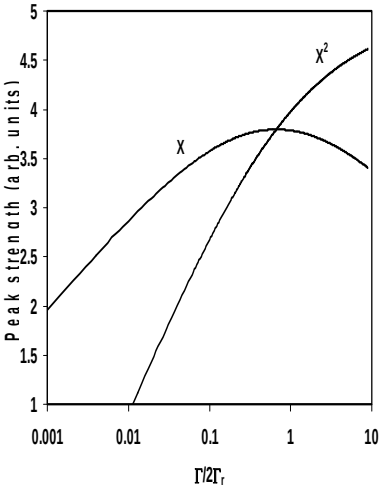

[Phys. Rev. B **69**, R41306 (2004)]

Quantum dot array(QDA) memory

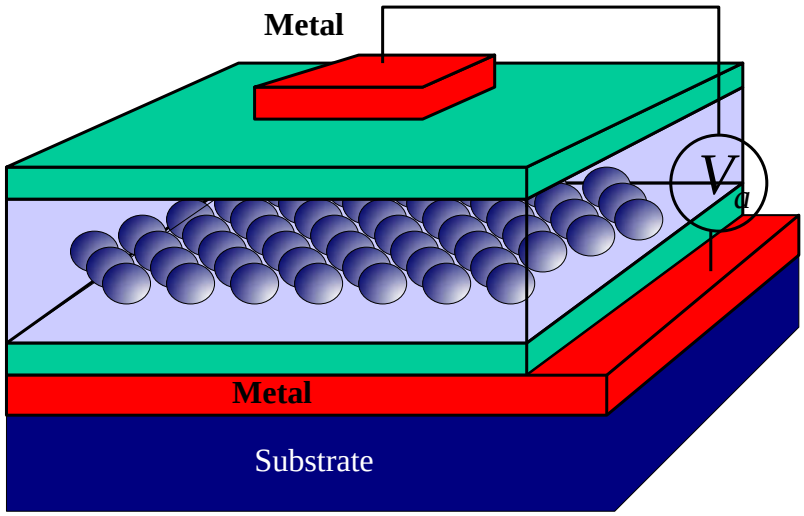

Coupling of degenerate p orbitals in QDA

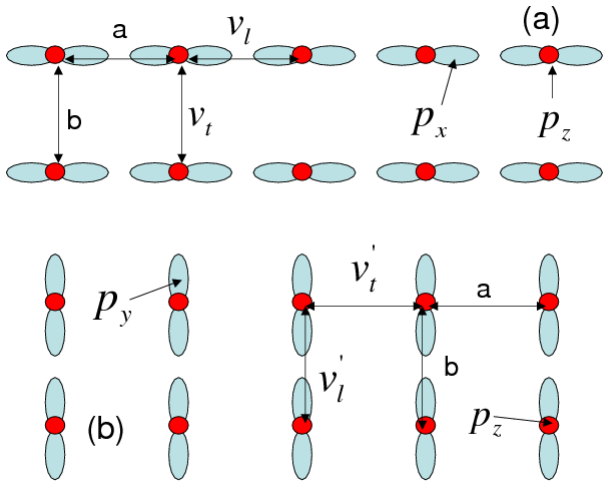

Bistable solution to occupation number

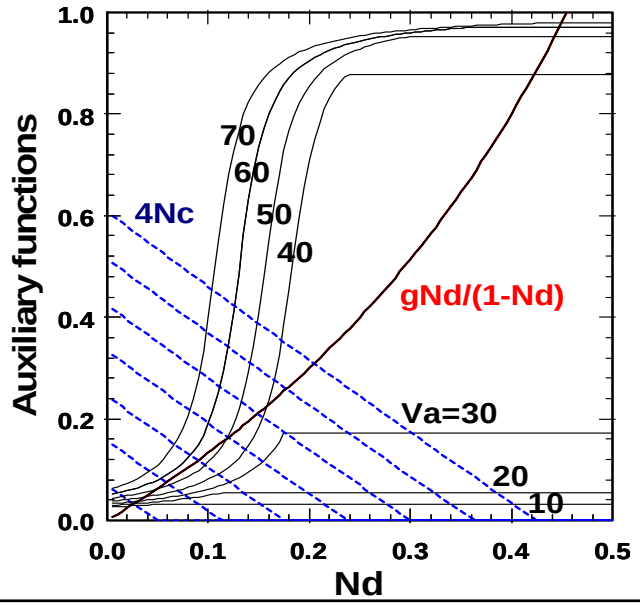

Bistable behavior of occupation number

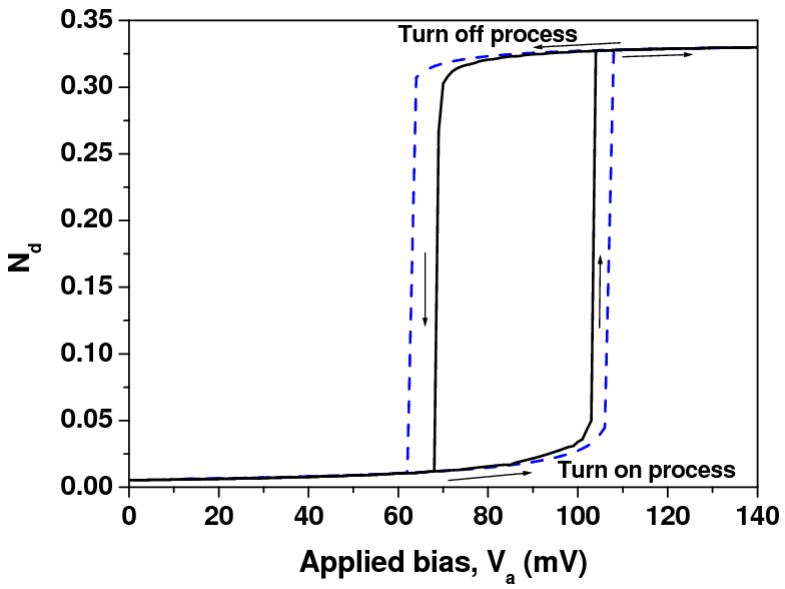

Bistable tunneling current through QDA

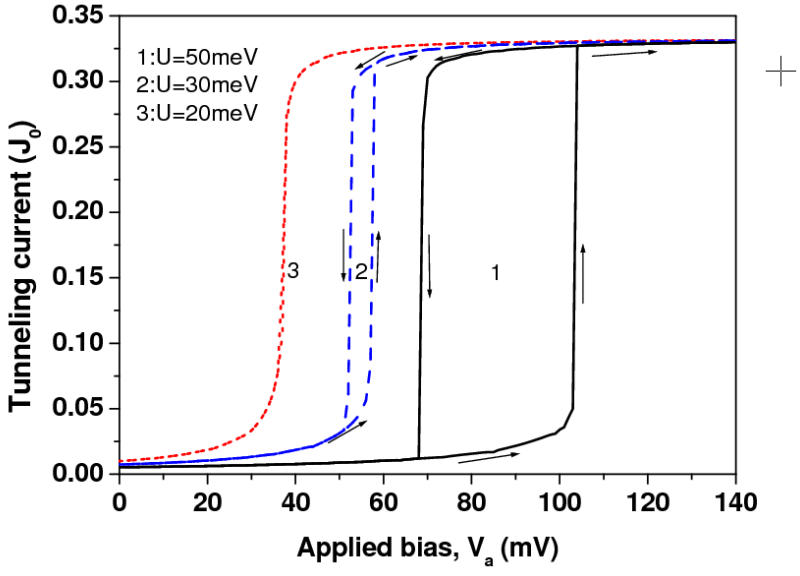

Bistable behavior of occupation number in the QDA bands

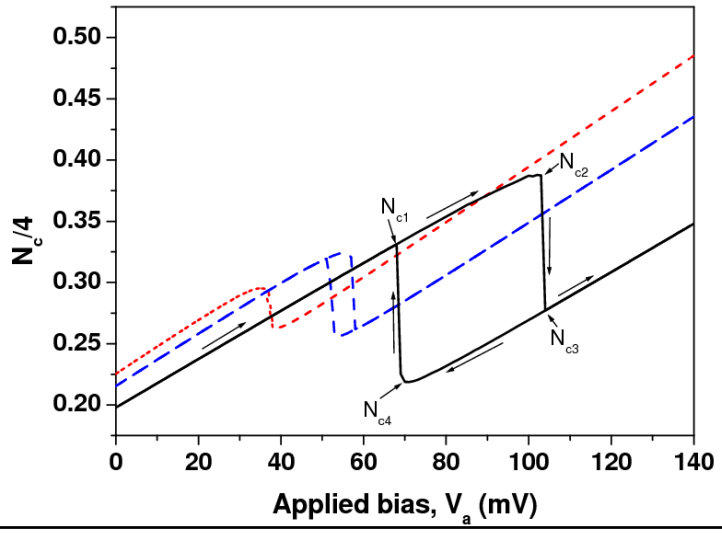

Bistable tunneling current from 2D to 1D

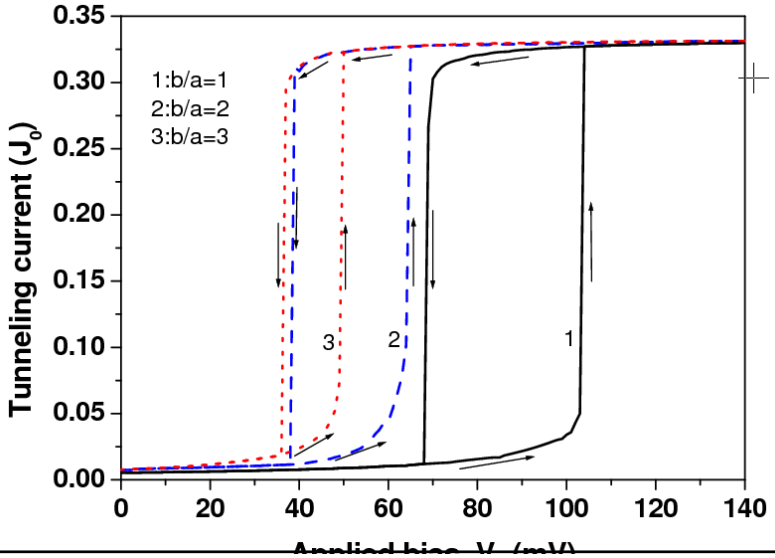

Effects of in/out ratio of tunneling rate in 1D QDA

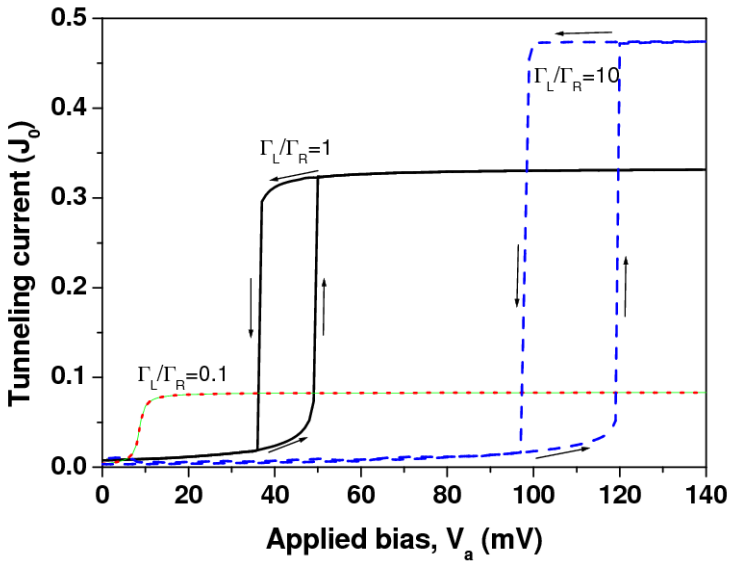

Summary

- **A simple, efficient and reliable closed-form formula is derived to reveal the tunneling current spectra of a complicated nanostructure junction**
- **Negative differential conductance arises from interdot Coulomb interactions**
- **The formula can also be used to study the transport properties of coupled nanostructures and QDA**
- **Memory effects of QDA with degenerate p orbitals are demonstrated**